Co-seismic Earthquake Lights: The Underlying Mechanism

Friedemann Freund

Pure and Applied Geophysics
pageoph

ISSN 0033-4553

Pure Appl. Geophys.
DOI 10.1007/s00024-019-02142-2

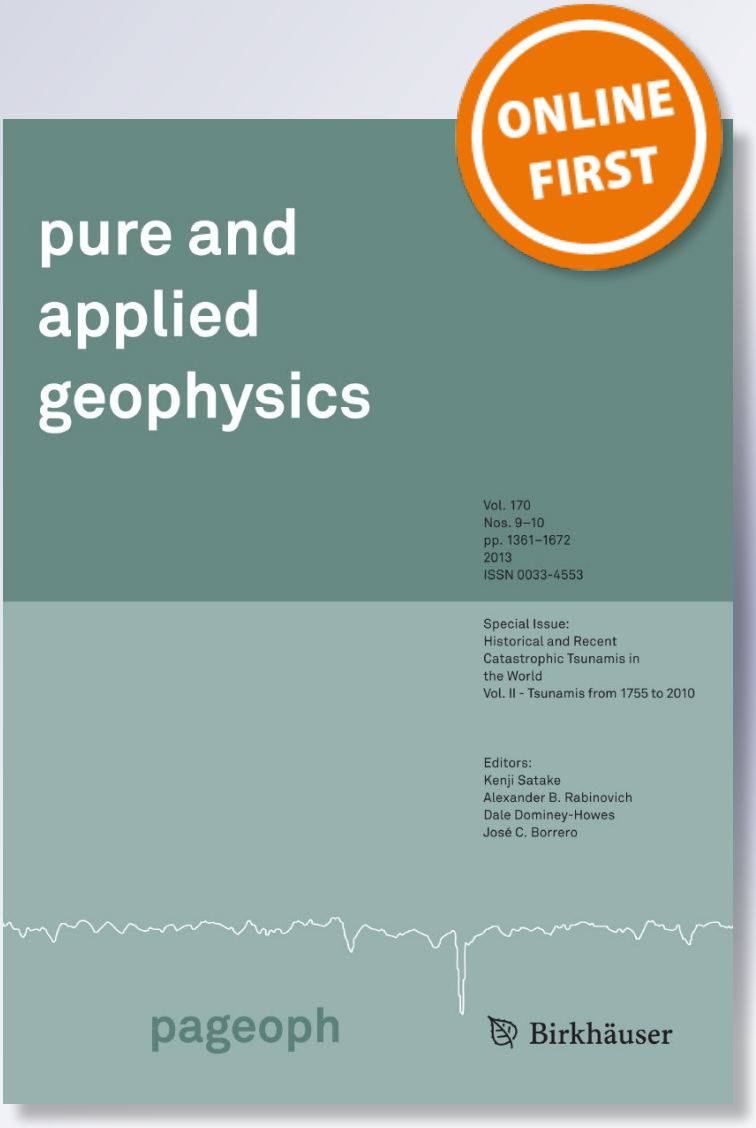

Springer

Pure Appl. Geophys.

https://doi.org/10.1007/s00024-019-02142-2

Pure and Applied Geophysics

Co-seismic Earthquake Lights: The Underlying Mechanism

Friedemann Freund[1,2,3,4]

Abstract—Earthquake lights (EQLs) have long been considered mysterious natural phenomena, for which no good physical explanation seemed to be available. Crucial to understanding EQLs, in particular the intense flashes of light bursting out of the ground while S waves propagate, is the presence of peroxy defects in igneous rocks, in particular in gabbroic rocks that typically fill the subvertical dykes in regions of past extensional tectonics. The peroxy defects tend to locate along grain boundaries or may even link adjacent mineral grains, making them highly susceptible to ever so slight displacements of mineral grains. Thus, the passage of an S wave will instantly activate peroxy bonds. If the number density of the stress-activated peroxy is so high that their delocalized wave functions overlap, the entire rock volume must instantly expand, supported from within by an electronic degeneration pressure. This process will be followed by a momentary dissociation of the peroxy defects, generating e′ and h· charge carriers, causing the volume to instantly contract again, at least partly. If an electric discharge can burst out from the top of the dyke, removing some of the charge carriers and generating an EQL, an additional volume contraction can be expected occur.

Key words: Earthquake lights, earthquake lightning, earthquake flashes, triboluminescence, piezoelectric, piezomagnetic, active faults, electric breakdown, arcing, flashover, transformer explosions.

1. Introduction

Anomalous luminous phenomena before, during and sometimes after major earthquakes have been reported for centuries, even millennia (Galli 1910; Milne 1911; Yasui 1973). They have been observed not only in epicentral regions, but sometimes also significant distances away from the epicenter, up to hundreds of kilometers (Papadopoulos 1999; Chen and Wang 2010). In the popular press they are often referred to as "mysterious" or "spooky". These luminous phenomena occur in different shapes, forms and colors, as diffuse airglows in the sky, as sudden outbursts of light from the ground, as cold flames licking up ankle-high, as luminous objects described as fiery pillars rising from the ground, as glowing balls floating through the air, and other rarer manifestations. A survey of historical reports found that the vast majority of these on earthquake-related luminosities, 97%, were associated with faults as most often found in rift or graben environments, which are formed during periods of extensional tectonics (Thériault et al. 2014). Such faults nearly always contain subvertical dykes, sheets of mafic rocks formed during extensional tectonics by the ascent of basaltic magmas from deep below, typically from > 100 km. These luminous phenomena are collectively known as earthquake lights (EQLs) (Derr 1973; Papadopoulos 1999). Though a number of hypothesis have been proposed the explain EQLs (Corliss 1982; Finkelstein et al. 1973; Finkelstein and Powell 1970; Lockner et al. 1983; Ouellet 1990; Johnston 1991; St-Laurent et al. 2006), how they are really generated is still largely shrouded in mystery.

This paper focuses on one subset of EQLs, the very short co-seismic outbursts of light from the ground, where "co-seismic" means that the EQLs are emitted as a seismic wave passes through some specific geological structures. When seismic waves from large seismic events travel through the ground, they have been observed to trigger flashes of light. These luminous outbursts typically last for only a fraction of a second. They involve electric discharges into the air (McMillan 1985). They appear to rise either from point sources or out of extended sources, probably along the traces of dykes. The EQLs can rise to considerable

[1] Carl Sagan Center, SETI Institute, Mountain View, CA 94043, USA. E-mail: friedemann.t.freund@nasa.gov
[2] GeoCosmo Science and Research Center, Los Altos, CA 94024, USA.
[3] NASA Ames Research Center, Moffett Field, CA 94035, USA.
[4] Department of Physics, San Jose State University, San Jose, CA 95192-0106, USA.

Published online: 11 March 2019

height above ground, on the order of 100 m or more, though the illumination of haze or low clouds by the intense light of these electric outbursts may lead to deceptively large estimates of true height.

Photographs of EQL flashes were obtained for the first time during the Matsushiro earthquake swarm near Nagano in Japan, when a very large number of medium and low magnitude earthquakes occurred within a two- year period, 1965–1967, triggering many EQL events (Matsushiro-Earthquake-Center 2000).

The photographic documentation of the Matsushiro EQLs led to a broader acceptance of the EQL phenomenon in the science community. Using the 6 April 2009 M = 6.3 L'Aquila earthquake in Italy as an example, Fidani reviewed a number of reports of lights reported in connection with earthquakes (Fidani 2010a). In recent years, since the widespread installation of closed-circuit surveillance cameras in urban and suburban areas, hundreds of EQL co-seismic flashes have been caught on video at many locations on different continents (Anonymous 2010; Fidani 2010b; Whitehead and Ulusoy 2015). An example is the M = 6.0 South Napa earthquake north of San Francisco, California, on Aug. 24, 2014, which struck during the night, at 03:20:44 local time. As the seismic waves propagated outward from the 11 km deep hypocenter, surveillance cameras recorded light flashes over a wide area, up to 200 km or more from the epicenter (Lamica 2014).

EQLs that resulted from the M = 8.0 earthquake of Aug. 15, 2007 in central Peru, about 25 km offshore the town of Pisco, at an epicentral depth 39 km, are particularly well-documented. This seismic event produced two main shocks, separated by about 75 s, and it hit at dusk at about 18:41 local time. The P wave and S wave trains took about 25 and 44 s respectively to reach Lima, 150 km to the NNW, where they were recorded by a seismometer station on the campus of PUCP and a co-located surveillance camera overlooking the Pacific Ocean towards the west (Heraud and Lira 2011). Figure 1 (top) and (center) show respectively the vertical ground acceleration and the mean ground acceleration calculated from the amplitudes of the vertical, N–S and E–W seismic signals. Figure 1 (bottom) depicts the intense flashes of light that were captured simultaneously by the surveillance camera. Frame-by-frame analysis of

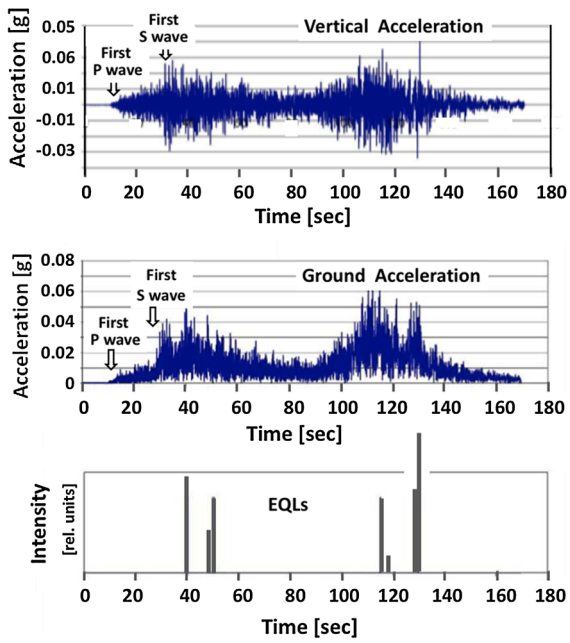

Figure 1
(Top): vertical ground acceleration at Lima, Peru, during the arrival of the P and S waves from the double shock M = 8 Pisco earthquake of Aug. 15, 2007; (Center): mean absolute ground acceleration obtained from the x–y–z components; (Bottom): seven outbursts of light from rocky outcrops on the coast as well as from offshore islets and the San Lorenzo Island were recorded in Lima during the passage of the S waves from the M = 8 Pisco earthquake 150 km to the SSE, after [24]

the video shows that there were no light flashes from the flat plane of Lima formed by sedimentary rocks. Instead the EQLs were emitted from bare rocks marking mafic dykes, including a cliff protruding into the Lima Bay, from several small rocky islets rising only a few meters above sea level and from the large San Lorenzo Island in front of Lima, about 8 km long and 2 km wide, which rises to nearly 400 m. The EQLs were emitted in the moment when the seismic waves intersected these dykes. The relative EQL intensities were estimated from the number of pixels on the CCD video camera that were saturated by the flashes.[1]

[1] Earthquake lights, including lightning flashes from the ground, seem to be limited to the presence of mafic dykes linked to extensional tectonics (Thériault et al. 2014). When EQLs are reported from areas where sedimentary rocks are prevalent at the surface, they may actually come from the top of geologically old dykes that are covered by sediments.

The timing of EQLs relative to the arrival times of the P waves and S waves shows that the light flashes are triggered by S waves, not by P waves. The difference between P waves and S waves is that S waves cause much more shear stresses. In a polycrystalline material like a rock, shear stresses primarily cause, on the microscale, displacements of grains relative to each other. In the case presented here, the EQLs were singular events occurring when the amplitudes of the seismic waves and resulting ground acceleration were high. The most intense light flash coincides with the strongest vertical acceleration near the 130 s mark.

In the past doubts have often been raised whether luminous phenomena reported in connection with earthquake activity, especially the light flashes, are due to natural processes or may be caused by exploding transformers or arcing high voltage–power lines (West 2017). Three arguments can be offered to alleviate these concerns:

1. There are numerous historical reports of luminous phenomena in connection with earthquake activity dating back to times well before electric transformers and high voltage–power lines. Hence, EQLs are definitely natural phenomena, even if—in modern times—exploding transformers or arcing high voltage–power lines add complexity,
2. EQLs like those recorded in Lima, Peru, cannot have come from transformers or high voltage–power lines because the camera was overlooking the ocean and documented light flashes from the uninhabited San Lorenzo Island as well as from small rocks rising barely above sea level, and
3. With high quality color video records, it is possible to spectroscopically distinguish true EQL outbursts from flashes of exploding transformers (Heraud and Lira 2011) and, with a larger error margin, also from flashes emitted by arcing power lines.

This paper presents a solid state mechanism that can account for burst-like electric discharges from deep within the ground, when powerful seismic waves intersect certain geological structures such as mafic dykes. This process leads to the prediction that, during the passage of the seismic wave, the rocks of the dyke must undergo a volume instability driven by the same electronic transition that drives the electric discharge. This volume instability establishes a link to the widely reported earthquake booms (USGS 2018), which will be the subject of a separate paper.

1.1. Discussion Basic Concept

The geological settings in and around Lima, Peru, and the observations depicted in Fig. 1 invite us to consider an S wave from a distant earthquake traversing a subvertical dyke. If the S wave arrives from a direction perpendicular to the plane of the dyke, it will cause the mafic rocks of the dyke to experience the same very rapid shear force over kilometers in width and depth. An S wave traveling at 3.4 km/s will traverse a 34 m thick dyke in 10 ms. Within this short time, electric charge carriers in the gabbroic rock forming the dyke become activated, a process for which we use the term “electrification”. In fact, the rocks in the dyke can become electrified to the point that they can produce a large electric discharge at the Earth surface. Three questions to be addressed are:

(1) How can a mafic dyke become electrified?
(2) Is it important that this process happens very fast?
(3) What is special about mafic rocks?

1.2. Insulator-Semiconductor Transition

Under normal conditions rocks are insulators, meaning that the band gap E_{gap} between the valence bands and the conduction bands of their constituent minerals is on the order of 4.5 eV or larger. Thus, the probability P to thermally promote electrons from the valence band into the conduction band becomes very small:

$$P \approx \exp -\left[E_g/kT\right]$$

where E_g, k and T are respectively the band gap E_{gap}, the Boltzmann constant and temperature in Kelvin. Between 300 and 600 K, kT is between 25 and 50 meV. If E_{gap} is on the order of 4.5 eV, P will be very small indeed, ranging from e-90 to e-180. However, all igneous rocks contain peroxy defects, i.e. tightly bonded pairs of oxygen anions that have converted from their common valence state-2 to the

valence state-1, hence, from O^{2-} to O^{-} such as in $O_3Si–OO–SiO_3$, where Si^{4+} may be substituted by Al^{3+} or other trivalent cations such as in feldspars (Freund and Freund 2015). From a semiconductor perspective a peroxy defect represents a self- trapped hole pair, $O^{-}–O^{-}$, where "hole" means a defect electron, here an O^{-} in a matrix of O^{2-}.

As long as the peroxy defect is intact, its two holes are localized forming a short, tight bond, and electrically inactive. However, the $O^{-}–O^{-}$ bond is subject to dissociation, when the Si-OO-Si entity is stressed in such a way that the Si-OO-Si bond angle deforms beyond some threshold value. The peroxy bond then dissociates in 2-steps as depicted in Fig. 2. The two dots in the center indicate the two holes that form the $O^{-}–O^{-}$ bond, which decouple during Step I, leading to the transition state. The one dot on the right indicates one hole remaining in the now broken peroxy bond after Step II, i.e. after an electron transfer has taken place from an outside O^{2-} into the decoupled peroxy bond. As a result, the donor O^{2-} becomes an O^{-}, i.e. an unbound hole h· in a matrix of O^{2-} (Scoville et al. 2015).

To further understand this 2-step process we look at the band structure as illustrated in Fig. 3. On the left, the peroxy defects are intact. Their presence is marked by dips in the energy surface of the valence band. The two antiparallel arrows indicate the tight diamagnetic spin pairing of the two electrons associated with the two O^{-} in the peroxy bond. During Step I, these electrons transition from a non-bonding molecular orbital into an antibonding molecular orbital, a process designated as "decoupling". In the decoupled state the wave functions associated with the antibonding orbital become delocalized, i.e. their spin density spreads over many neighboring O^{2-} while still maintaining their antiparallel, diamagnetic state as indicated in the center of Fig. 3 (Batllo et al. 1991). During Step II, an electron is transferred from an outside O^{2-} into the decoupled $O^{-}–O^{-}$ bonds, equivalent to dissociation. While the donor O^{2-} turns into an unbound O^{-}, also with a delocalized electronic wave function, the transferred electron becomes trapped on shallow energy levels below the upper edge of the valence band. Because of the wave nature of the electronic states below the edge of the valence band, they are mirrored by energy levels above the edge of the valence band as indicated on the right side of Fig. 3. The generation of e′ and h· charge carriers marks the transition from an insulator to a semiconductor state, i.e. to the onset of electronic conductivity, a process described by the term "electrification".

Here, a brief review is in order describing what is already known about the e′ and h· charge carriers. Thee′ become localized in the shallow traps indicated on the right of Fig. 3. These energy levels are available only where peroxy defects have been activated. These energy levels are not available outside the volume in which the activation has taken place. If stresses have done it, the holes h· generated during Step II have the remarkable ability to flow out of the stressed rock volume into the surrounding less stressed or unstressed rocks. Since the valence bands of minerals inside the stressed rock volume are electrically connected via their covalent component to the valence bands of other minerals, the holes can propagate along the upper edge of the common valence band. The distance over which holes h· can propagate is, in principle, unlimited, while the e′ are

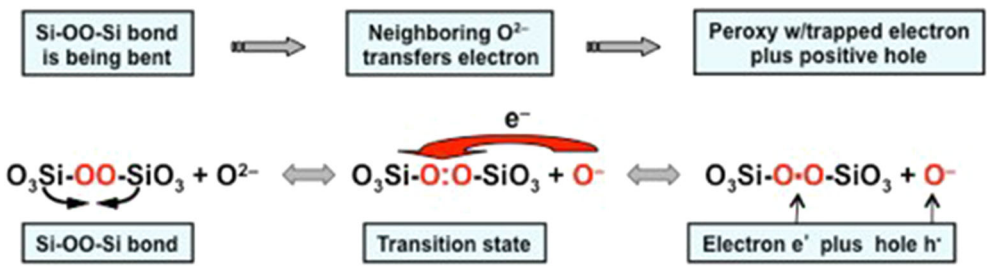

Figure 2
Activation of the peroxy bond in a silicate matrix via a 2-step process that leads to an electron–hole pair, e′ and h·, in the oxygen sublattice

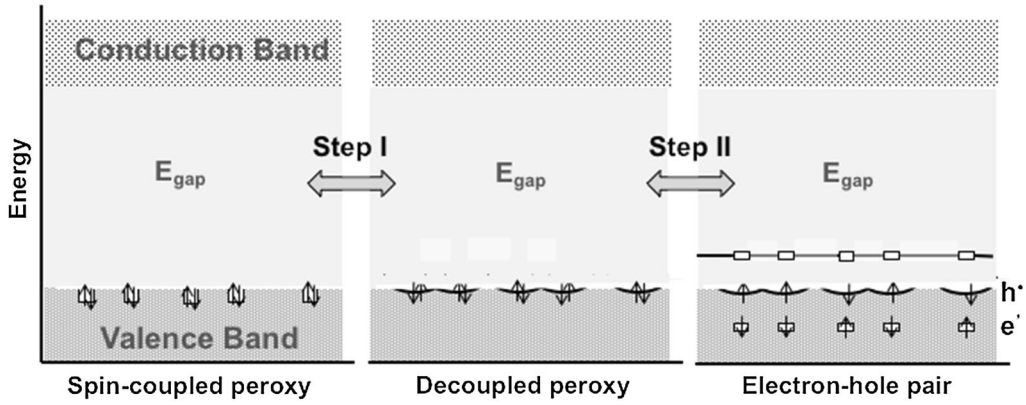

Figure 3
Simplified representation of the band structure of an insulator that contains peroxy defects. Left: self-trapped hole pairs in the O^{2-} sublattice creating dips in the energy surface associated with O 2sp energy levels. Center: Decoupling of the hole pairs and concomitant delocalization of the wave functions of the hole states. Right: dissociation of the hole pairs, trapping of the electrons in energy levels slightly below the edge of the valence band and generation of unbound hole states at the edge of the valence band

restricted in their mobility to the stressed rock volume.

In a number of publications over several years (Freund et al. 1990, 1994, 2006; Bortnik et al. 2010; Scoville et al. 2015), it has been demonstrated that stress-activated $h^{\cdot}$ charge carriers readily spread into adjacent less stressed or unstressed rocks. Their mode of propagation is thought to involve phonon-assisted electron hopping, a mechanism that is consistent with their experimentally determined speed of propagation, $\sim$ 100 m/s.

1.3. *Lifetimes of the Stress-Activated Charge Carriers*

There is another factor that controls the $h^{\cdot}$ outflow. The number of $h^{\cdot}$, which can flow out from a given rock volume, is given by the number of e' and $h^{\cdot}$ activated within a given time interval and the rate, at which the e' and $h^{\cdot}$ recombine inside that volume, returning to the inactive peroxy state. The faster the stresses are applied, the larger number of e' and $h^{\cdot}$ activated. At the same time the e' and $h^{\cdot}$ start to recombine. Thus, the number of $h^{\cdot}$ in the rock volume that are available to flow out is given by the difference between the rate of activation and the rate of recombination. By recording the h* outflow from a rock volume stressed at different rates we can obtain information about the lifetimes of the $h^{\cdot}$ charge carriers.

Figure 4a and c were derived from a set of experiments with a 30 × 30 × 0.9 cm^3 tile of a fine-grained black gabbro from Shanxi, China, stressing a cylindrical volume of about 10 cm^3 in the center and measuring the current flowing to the outer rim of the tile. Maintaining this geometry, the stress rates were varied over more than 5 orders of magnitude. Figure 4a, b demonstrate that the outflow currents increase exponentially with the increase of the rate of stressing. Plotting the currents on a log–log scale in pA cm^{-3} versus the time of the maxima leads to two exponential straight sections as shown in Fig. 4c, indicating a wide distribution of lifetimes of the stress-activated e' and $h^{\cdot}$ charge carriers and two recombination mechanisms. Low impact velocity experiments have provided additional information that the exponential relation between the rate of stressing and the amount of outflow current extends into the submillisecond range (Scoville et al. 2015).

The implication of these experiments is that, when a rock that contains a high concentration of peroxy defects is stressed very rapidly such as during the passage of a broadside S wave hitting a mafic dyke, a very large number of its peroxy defects become near-instantly activated. However, before breaking up and releasing e' and $h^{\cdot}$, they must go through an electronic transition, which is coupled to a very fast volume increase, followed by an equally fast volume contraction. As will be discussed in more detail below, this rapid succession of volume changes is part of the

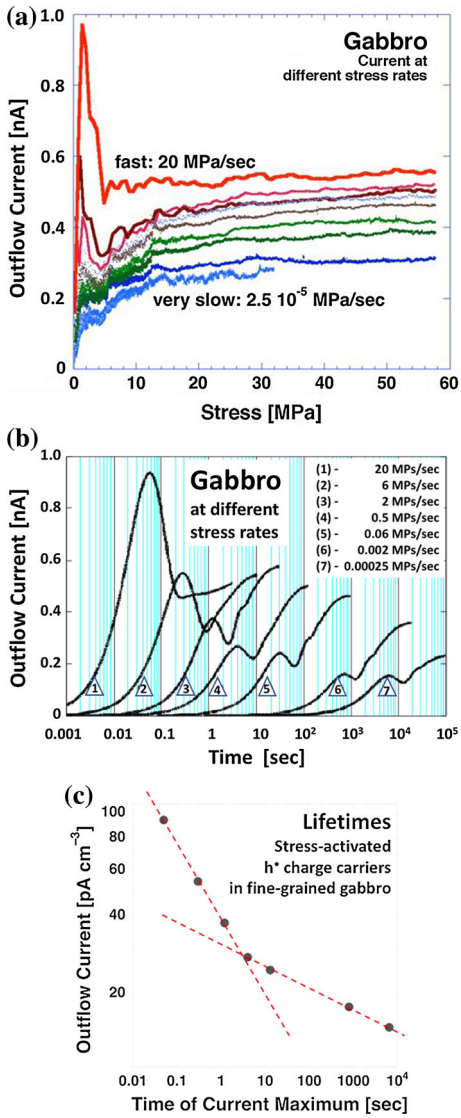

Figure 4
a Outflow currents from a gabbro tile loaded in the center ($\sim$ 10 cm^3) at different rates, plotted as a function of the stress up to 58 MPa. **b** Same outflow currents as in **a** plotted as current versus log time. **c** Log–log plot of the outflow current versus time of the first outflow maximum

electrification of the rock and linked to the electric discharge into the air.

1.4. Delocalization and Overlap of the Wave Functions

Semiconductor band theory postulates that electrons promoted from the valence band to the conduction band are no longer attached to single atoms, i.e. localized, but enter a delocalized state whereby they are enabled to move throughout the entire solid. They behave like a "sea of electrons" which can surge throughout the solid medium, forming an electrical current. The electrons in the valence bands of semiconductors can cross grain boundaries, and move from grain to grain, even between grains of different structure and composition.

Though the concept of delocalized wave functions has been developed for electrons in semiconductors, it also holds true for hole charge carriers in insulators, if they are associated with energy levels at the top of the valence band (Li et al. 2012). This fact was recognized early during the study of peroxy defects in MgO and their effect on a range of physical properties including electrical conductivity (Kathrein and Freund 1983), thermal expansion (Wengeler and Freund 1980), dielectric and paramagnetic susceptibility (Freund et al. 1990, 1996; Batllo et al. 1990), refractive index (Freund et al. 1994) and mechanical properties (Freund et al. 2010). It provided the basis for understanding the presence of hole states not only in MgO, but also in a broader range of materials and in minerals up to igneous and high-grade metamorphic rocks, in which peroxy defects are ubiquitous and omnipresent (Freund and Freund 2015).

When the number density of peroxy defects becomes so high that, upon activation, their wave functions overlap, a different situation arises. Overlapping wave functions mean that the previous semiconductor state turns into a quasi-metallic state, marked by a dramatic increase in electrical conductivity. Noting that the highest number densities of stress-activated e′ and h· charge carriers are available only for a short time, due to their rapid recombination, we can expect that a dyke traversed by an S wave will be only very briefly in an electrified state. In other words, the mafic rocks of the dyke will suddenly become highly conductive and then quickly return to their non-conductive state.

The question then arises whether the mere fact that the rocks in the dyke become electrified will cause an electrical discharge from the top of the dyke. Intuitively, a sudden increase in conductivity of the rocks should not—on its own merits—lead to an

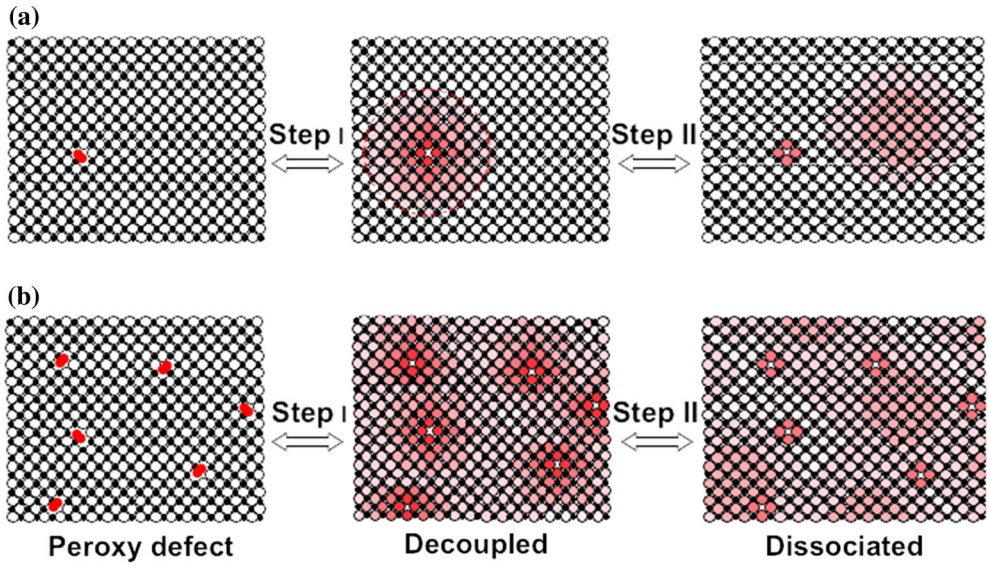

Figure 5
a Two-step break-up of the peroxy bond, here shown in the cubic matrix of MgO, leading to the decoupled state and, thence, the dissociated states. **b** If the number density of peroxy defects is high, the wave functions of their hole states will overlap, both upon decoupling and dissociation, leading to a quasi-metallic state

electric discharge. What seems to be still missing is some sort of driving force that would initiate a dielectric breakdown from the top of the dyke.

1.5. Volume Change During Peroxy Activation

Further insight can be gained by considering the processes on the atomic scale, specifically the changes in the electronic structure of the peroxy defects during the Step I and Step II transitions as depicted in Fig. 5a, b. Molecular Orbital (MO) theory is a helpful tool.

Figure 6 presents the MO diagram of the O_2^{2-} anion, the simplest peroxy defect as it occurs in the cubic lattice environment of MgO. On the left and right are the atomic orbitals (AOs) for O^-. The center shows the MOs derived from the linear combination of the O $2s^2$ and O $2p^4$ AOs, plotted on an arbitrary energy scale (Chen and Chang 1998). The two highest MOs (circled in red) are the occupied, fourfold degenerate 1 π_g^x and 1 π_g^y orbitals, which are non-bonding, and the $3\sigma_u^*$ orbital, which is antibonding but unoccupied. In the Highest Occupied Molecular Orbital (HOMO), the non-bonding $1\pi_g^x$–$1\pi_g^y$ level, the electron density is concentrated in the torus around the O^-–O^- bond formed by the O $2\pi_x$ and $2\pi_y$ AOs. The absence of electron density in the Lowest Unoccupied Molecular Orbital (LUMO), the antibonding $3\sigma_u^*$ level, allows the intact O^-–O^- bond to be very short, < 1.5 Å (Edwards and Fowler 1982; Ricci et al. 2001). However, this electronic configuration is sensitive to displacements of the atoms relative to each other such as caused by thermal vibrations during heating (Freund and Masuda 1991) or mechanical displacements by deviatoric stresses.

To illustrate what happens when the peroxy bond is perturbed by deviatoric stresses, we move on to the $O_3Si/^{OO}\backslash SiO_3$ entity as depicted at the upper part of Fig. 7. For the sake of illustration, we keep the same group-theoretical designations π and σ as for the MOs of the peroxy anion, O_2^{2-}. When the $O_3Si/OO/SiO_3$ entity is stressed and the angle α changes, the fourfold degeneracy of the non-bonding MO's $1\pi_g^x$ and $1\pi_g^y$ is lifted. If the plane of the drawing is taken as the xz plane, changing the angle α causes the energy of the in- plane MO to be raised and the energy of the orthogonal out-of-plane MO to be lowered. Inevitably, at some threshold value of α, the in-plane $1\pi_g$ must cross the antibonding $3\sigma_u^*$, forcing

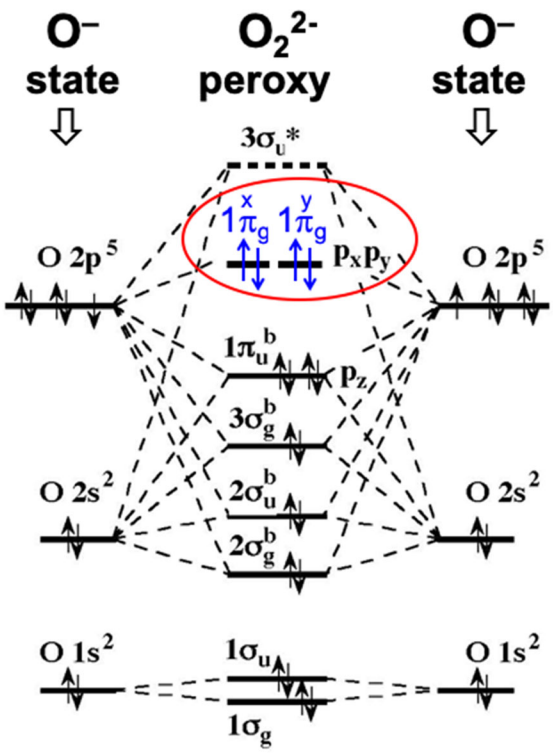

Figure 6
Molecular orbital diagram of the peroxy anion with its highest energy level, the antibonding σ-type level, being empty. This allows the O^-O^- bond to be very short

the two electrons from the non- bonding π-type MO into the anti-bonding σ-type MO. As a result, electron density that had resided in the tight torus around the axis of the O^-–O^- bond is transferred into the antibonding region, pulling the two O^- apart, causing (1) decoupling and (2) dissociation. Both crossing points are marked by red circles.

During decoupling, the O^-–O^- bond distance nearly doubles, from < 1.5 Å, to a value closer to that of the interatomic distances between O^{2-}, 2.8–3.0 Å. At the same time, because the electrons transition from the non- bonding $1\pi_g^{xy}$ MOs into the antibonding $3\sigma_u^*$ MO, the volume of the two decoupled O^- expands by a factor of about 8. During the next step, dissociation of the peroxy bond, an electron is transferred from an outside donor O^{2-} into the O^-–O^- bond. While this e′ becomes trapped in the peroxy bond, the donor O^{2-} turns into O^-, hence an h·, which is unbound and becomes a mobile charge carrier.

During this sequence, during Step I, the size of the two O^- increases as indicated in the lower part of Fig. 7. During Step II, dissociation, the volume partly contracts again. This sequence of events on the atomic scale affects what happens on the macroscale, in the Earth's crust, when a powerful S wave hits a subvertical dyke broadside. Assume that the dyke reaches down 40–50 km and its rocks contain enough peroxy defects so that, upon decoupling, their wave functions will overlap as depicted for Step I for Fig. 5b. Travelling at $\sim$ 3.4 km/s, the S wave will shear the entire rock sheet simultaneously within milliseconds. As the peroxy bonds decouple, the rock volume must expand. In a laterally confined sheet of rock extending down 40–50 km trying to expand within milliseconds, a large overpressure is expected to develop, supported from within by the electron degeneration pressure of the overlapping wave functions (Liboff 1984).

1.6. Electric Discharge Driven by Volume Contraction

Once the peroxy defects are decoupled, all it takes to break them apart is an electron transfer from a neighboring O^{2-} as depicted on the right in the upper part of Fig. 7. In that instant mobile e′ and h· charge carriers are created, causing the mafic dyke rock to enter a plasma-like state. At the same time, as Step II in Fig. 5b and the lower part of Fig. 7 illustrate, the volume contracts. This volume contraction can be viewed as a rebound, during which some of the internal pressure is relieved that Step I had created. The rebound is expected to be able to go further, at least incrementally, if some of the activated electronic charge carriers were removed from the system.

In principle the charge carriers could flow out laterally from the dyke rock into the embedding rocks. However, as stated above, dykes are usually embedded into sedimentary rocks that do not contain sufficiently high concentrations of peroxy defects to achieve this state of short-lived degeneracy that is a prerequisite for high conductivity and would allow the activated charge carriers in the dyke rock to leak out laterally from the dyke within milliseconds.

Hence, the only direction for the charge carriers is upward. The ejection from the top of the dyke is

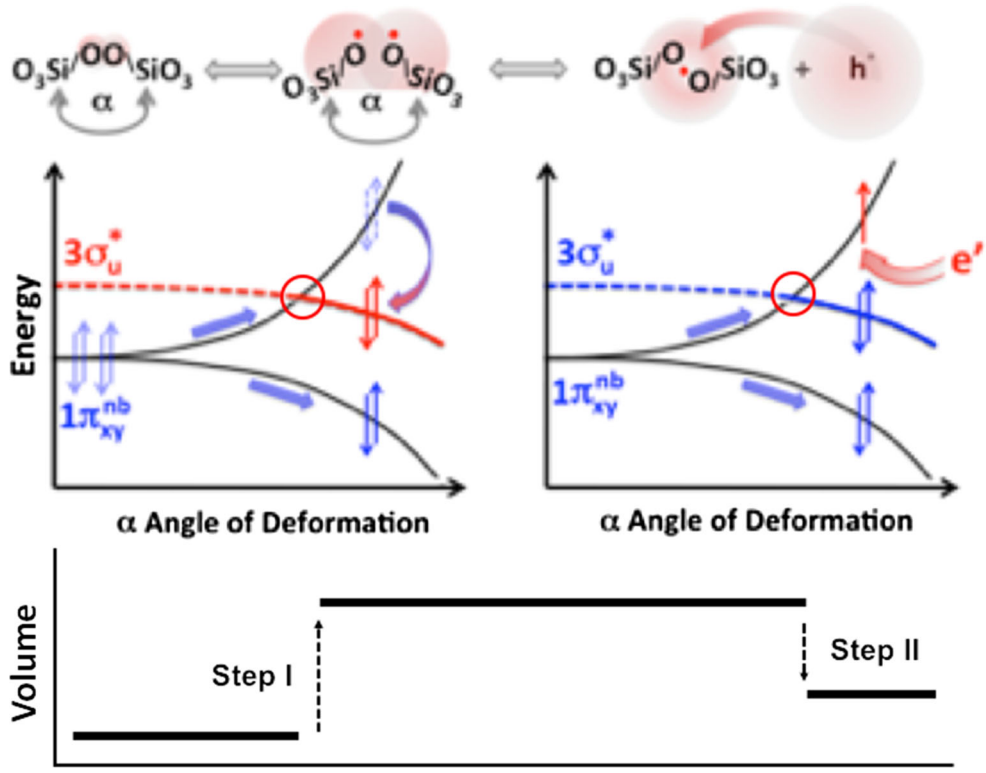

Figure 7
Representation of the two highest MO levels of $O_3Si/OO\backslash SiO_3$ during deformation of the peroxy bond angle. The fourfold degenerate non-bonding p-type level will split. At a critical angle α, one MO will cross the σ* level, causing two electrons to transition into the antibonding orbital. In that moment the diameter of the two O^- increases by a factor of nearly 2

possible because, once the rock has entered the plasma-like state, the impulse created by the onset of a discharge can propagate downward very fast, at the speed of light divided by the dielectric constant (Diaz et al. 2015), allowing the discharge to extract charge carriers from deep below very, thereby "feeding" the EQL.

Figure 8 summarizes this scenario when an S wave impacts a vertical dyke at right angle. Assuming that the dyke rock contains enough peroxy defects to allow the electronic wave functions of the decoupled peroxy bonds to overlap, the rock volume will very rapidly expand, supported by the electron degeneration pressure. This volume expansion will place even if the rock is under high compressive stress as indicated by the short gray arrows perpendicular to the dyke. The Step I volume expansion will be immediately followed by a partial volume contraction during Step II, when peroxy bonds break up generating e′ and h· charge carriers. This Step II will cause the rock to become quasi-metallic.

An additional volume contraction is thought to be possible when charge carriers are removed from the system as indicated the long vertical gray arrow in Fig. 8. This sequence of very rapid events concludes with the forceful plasma ejection across the rock-air interface, which constitutes an EQL.

2. *Conclusions*

Earthquake lights (EQLs) have long been considered mysterious natural phenomena, for which no good physical explanation seemed to be available. EQLs include the flashes of light bursting out of the surface of the Earth, while seismic waves from large earthquakes propagate through the ground. Observational evidence suggests that these outbursts of light

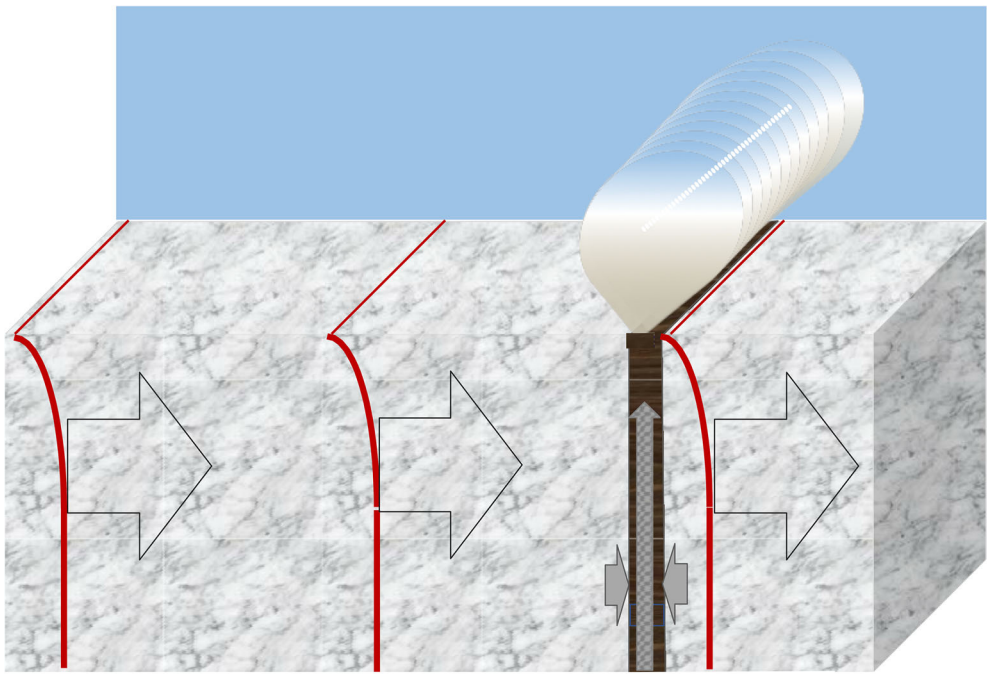

Figure 8
Schematic representation of an S wave traveling from left to right, hitting a vertical dyke from the broadside. The gray vertical arrow in the dyke indicates the millisecond volume expansion across the entire dyke sheet, which leads to a strong internal stress plus a compressive stress component exerted by the embedding rocks. The volume expansion is followed by a volume contraction, which accompanies the generation of e′ and h· charge carriers. The sequence concludes with the forceful plasma ejection across the rock-air interface

occur preferentially, probably exclusively, in regions marked by the presence of subvertical dykes due to past extensional tectonics (Thériault et al. 2014).

Crucial for understanding the underlying physical processes is the presence of peroxy defects in the igneous rocks that form the dykes, primarily mafic rocks such as gabbros (Freund and Freund 2015; Scoville et al. 2015; St-Laurent et al. 2006). Since peroxy defects tend to sit along grain boundaries or may link adjacent mineral grains, they are highly susceptible to ever so slight displacements of mineral grains relative to each other. Thus, the shear forces exerted by S waves can be expected to be highly effective in straining the $O_3Si/OO\backslash SiO_3$ bond angle, initiating the 2-step activation of the peroxy bonds. If the number density of the peroxy defects per unit volume of rock is high enough to allow their delocalized wave functions to overlap, the volume of the dyke rock must instantly expand during Step I of the decoupling of the peroxy defects, instantly followed by Step II, dissociation, during which e′ and h· charge carriers are generated and the volume partly contracts again. A further incremental volume decrease is expected to occur, when an electric discharge occurs from the top of the dyke, generating an EQL.

Acknowledgements

I thank an anonymous reviewer tor very insightful comments and suggestions. This study draws on work that was supported by the NASA Ames Research Center through several "Director's Discretionary Fund" (DDF) grants, by the NASA "Earth Surface and Interior" (ESI) Grant 2010 NNX08AG81G_S03, and through a Goddard Earth Science and Technology (GEST) Fellowship at the Geodynamics Branch, NASA Goddard Space Flight Center. I thank Dr. Bobby SW Lau and Dr. Akihiro Takeuchi for their contributions to the experimental work. I thank Professor Charles W. Schwartz, Department of Civil

and Environmental Engineering, University of Maryland, for laboratory support.

References

Anonymous. (2010). Registran enormes luces en el cielo durante terremoto de 8.8 grados de magnitud que destruyó Chile, in *Actualidad*, Lima, Peru. https://web.archive.org/web/20100301224159/http://www.peru.com/noticias/portada20100228/83581/Registran-enormes-luces-en-el-cielo-durante-terremoto-de-88-grados-de-magnitud-que-destruyo-Chile.

Batllo, F., LeRoy, R. C., Parvin, K., & Freund, F. (1990). Dissociation of O_2^{2-} defects into paramagnetic O^- in wide band gap insulators: a magnetic susceptibility study of magnesium oxide. *Journal of Applied Physics, 67,* 588–596. https://doi.org/10.1063/1.345984.

Batllo, F., LeRoy, R. C., Parvin, K., Freund, F., & Freund, M. M. (1991). Positive hole centers in MgO—Correlation between magnetic susceptibility, dielectric anomalies and electric conductivity. *Journal of Applied Physics, 69,* 6031–6033. https://doi.org/10.1063/1.347807.

Bortnik, J., Bleier, T. E., Dunson, G., & Freund F. (2010). Estimating the seismotelluric current required for observable electromagnetic ground signals. *Annales Geophysicae 28,* 1625–1624. https://doi.org/10.5194/angeo-28-1615-2010.

Chen, E.-H., & Chang, T.-C. (1998). Walsh diagram and the linear combination of bond orbital method. *Journal of Molecular Structure: THEOCHEM, 431,* 127–136. https://doi.org/10.1016/S0166-1280(97)00432-6.

Chen, Q.-F., & Wang, K. (2010). The 2008 Wenchuan earthquake and earthquake prediction in China. *Bulletin of the Seismological Society of America, 100*(58), 2840–2857. https://doi.org/10.1785/0120090314.

Corliss, W. R. (1982). *Lightning, Auroras, Nocturnal Lights: A Catalog of Geophysical Anomalies*. The Sourcebook Project, Glen Arm, MD. 248 pages, 74 illustrations, 1070 refs. ISBN 915554-09-7.

Derr, J. S. (1973). Earthquake lights: a review of observations and present theories. *Bulletin of the Seismological Society of America, 63,* 2177–2187.

Diaz, A., Friedman, J. S., Luciano, S., Martinez, S., Hernandez, A., de Jesus, J., & Maldonado, P. M. (2015). Propagation of Electromagnetic Waves through Homogeneous Media, paper DTE06 presented at ETOP Meeting of the Optical Society of America.

Edwards, A. H., & Fowler, W. B. (1982). Theory of the peroxy-radical defect in a-SiO_2. *Physical Review, 26,* 6649–6660.

Fidani, C. (2010a). The earthquake lights (EQL) of the 6 April 2009 Aquila earthquake in Central Italy. *Natural Hazards and Earth System Sciences, 10,* 967–978. https://doi.org/10.5194/nhess-10-967-2010.

Fidani, C. (2010b). *ELF signals by Central Italy electromagnetic network in 2008–2010, paper presented at GNGTS-Gruppo Nazionale di Geofisica della Terra Solida*. Italy: Trieste.

Finkelstein, D., Hill, U. S., & Powell, J. R. (1973). The piezoelectric theory of earthquake lightning. *Journal of Geophysical Research, 78,* 992–993.

Finkelstein, D., & Powell, J. (1970). Earthquake lightning. *Nature, 228,* 759–760.

Freund, F., Batllo, F., & Freund M. M. (1990). Dissociation and recombination of positive holes in minerals. In L. M. Coyne, S. W. S. McKeever & D. F. Blake (Eds.), *Spectroscopic characterization of minerals and their surfaces* (pp. 310–329). American Chemical Society, 390 https://doi.org/10.1021/bk-1990-0415.ch016.

Freund, F. T., & Freund, M. M. (2015). Paradox of Peroxy Defects and Positive Holes in Rocks, Part I: Effect of Temperature. *Journal of Asian Earth Sciences, 2015,* 373–383. https://doi.org/10.1016/j.jseaes.2015.04.047.

Freund, M. M., Freund, F., Butow, S., Korvink, J. G., & Baltes, H. (1996). *Hole injection into MgO from self-trapped positive hole pairs, paper presented at American Physical Society*. APS, St. Louis, MO, USA: Annual March Meeting.

Freund, F. T., Hoenig, S. A., Braun, A., Momayez, M., & Chu, J. J. (2010). *Softening rocks with stress activated electric current, paper presented at 5th International Symposium on In-situ Rock Stress (ISRSV)*. China: Beijing.

Freund, F., & Masuda, M. M. (1991). Highly mobile oxygen hole-type charge carriers in fused silica. *Journal of Materials Research, 6*(8), 1619–1622. https://doi.org/10.1557/JMR.1991.1619.

Freund, F. T., Takeuchi, A., & Lau, B. W. (2006). Electric currents streaming out of stressed igneous rocks—A step towards understanding pre-earthquake low frequency EM emissions. *Physics and Chemistry of the Earth, 31,* 396–399.

Freund, F., Whang, E.-J., Batllo, F., Desgranges, L., Desgranges, C., & Freund, M. M. (1994). Positive hole– type charge carriers in oxide materials. In L. M. Levinson & S.-I. Hirano (Eds.), *Grain boundaries and interfacial phenomena in electronic ceramics* (pp. 263–278). Amer. Ceram. Soc.: Cincinnati, OH.

Galli, I. (1910). Raccolta e classificazione dei fenomeni luminosi osservati nei terremoti. *Bolletino della Societa Sismological Italiana, 14,* 221–448.

Heraud, J. A., & Lira, J. A. (2011). Co-seismic luminescence in Lima, 150 km from the epicenter of the Pisco, Peru earthquake of 15 August 2007. *Natural Hazards and Earth System Sciences, 11,* 1025–1036.

Johnston, A. C. (1991). Light from seismic waves. *Nature, 354*(6352), 361. https://doi.org/10.1038/354361a0.

Kathrein, H., & Freund, F. (1983). Electrical conductivity of magnesium oxide single crystal below 1200 K. *Journal of Physics and Chemistry of Solids, 44,* 177–186.

Lamica, C. (2014). Earthquake lights Santa Rosa/Napa earthquake, https://www.youtube.com/watch?v=RknvjVTCFhM.

Li, K., Kang, C., & Xue, D. (2012). Relationship between band gap and bulk modulus of semiconductor materials. *Materials Focus, 1*(1), 88–92. https://doi.org/10.1166/mat.2012.1014.

Liboff, R. L. (1984). Criteria for physical domains in laboratory and solid-state plasmas. *Journal of Applied Physics, 56*(9), 2530–2535.

Lockner, D. A., Johnston, M. J. S., & Byerlee, J. D. (1983). A mechanism for the generation of earthquake lights. *Nature, 302,* 28–33.

Matsushiro-Earthquake-Center. (2000). Catalogue of literature and documents on the Matsushiro Earthquake Swarm. https://dil-opac.bosai.go.jp/publication/nied_tech_note/pdf/KJ-01_198.pdf.

McMillan, W. G. (1985). Earthquake light. In *Final Report, 1 Mar. 1983–15 Aug. 1986 McMillian Science Associates, Inc., Los Angeles, CA. Rep. AD-A61385* (p. 53). Geophysics/STI, Los Angeles.

Milne, J. (1911). Earthquakes and Luminous Phenomena. *Nature, 87*(2175), 16.

Ouellet, M. (1990). Earthquake light and seismicity. *Nature, 348*(6301), 492.

Papadopoulos, G. (1999). Luminous and fiery phenomena associated with earthquakes in the East Mediterranean. In M. Hayakawa (Ed.), *Atmospheric and ionospheric electromagnetic phenomena associated with earthquakes* (pp. 559–575). Tokyo: Terra Scientific Publishing.

Ricci, D., Pacchioni, G., Szymanski, M. A., Shluger, A. L., & Stoneham, A. M. (2001). Modeling disorder in amorphous silica with embedded clusters: The peroxy bridge defect center. *Physical Review B, 64*(22), 224104–224108.

Scoville, J., Sornette, J., & Freund, F. T. (2015). Paradox of peroxy defects and positive holes in rocks Part II: Outflow of electric currents from stressed rocks. *Journal of Asian Earth Sciences, 114*(Part 2), 338–351. https://doi.org/10.1016/j.jseaes.2015.04.016.

St-Laurent, F., Derr, J., & Freund, F. (2006). Earthquake lights and the stress-activation of positive hole charge carriers in rocks. *Physics and Chemistry of the Earth, 31*(4–9), 305–312.

Thériault, R., St-Laurent, F., Freund, F., & Derr, J. (2014). Prevalence of earthquake lights associated with rift environments. *Seismological Research Letters, 85*(1), 159–178. https://doi.org/10.1785/0220130059.

USGS. (2018). Earthquake Booms, Seneca Guns, and Other Sounds. https://earthquake.usgs.gov/learn/topics/booms.php.

Wengeler, H., & Freund, F. (1980). Atomic carbon in magnesium oxide, Part III: Anomalous thermal expansion behavior. *Materials Research Bulletin, 15*(9), 1241–1245. https://doi.org/10.1016/0025-4395408(80)90026-4.

West, M. (2017). Explained: Mexico City Earthquake Lights [Power Line Arcing and Transformer Explosions], Metabunk.org; https://www.metabunk.org/explained-mexico-city-earthquake-lights-power-line-arcing-and-transformer-explosions.t9044/.

Whitehead, N. E., & Ulusoy, U. (2015). Origin of earthquake light associated with earthquakes in Christchurch, New Zealand, 2010–2011. *Earth Sciences Research Journal, 19*(2), 113–120. https://doi.org/10.15446/esrj.v19n2.47000.

Yasui, Y. (1973). A summary of studies on luminous phenomena accompanied with earthquakes. *Memoirs Kakioka Magnetic Observatory, 15*(2), 127–138.

(Received September 23, 2018, revised February 4, 2019, accepted February 22, 2019)